


# Hierarchical lichee-like $Fe_3O_4$ assemblies and their high heating efficiency in magnetic hyperthermia

Wen-Yu Li(李文宇), Wen-Tao Li(李文涛), Bang-Quan Li(李榜全), Li-Juan Dong(董丽娟), Tian-Hua Meng(孟田华), Ge Huo(霍格), Gong-Ying Liang(梁工英), and Xue-Gang Lu(卢学刚)

**Citation:**Chin. Phys. B, 2021, 30 (**10**): 104402. DOI: 10.1088/1674-1056/ac0789
Journal homepage: http://cpb.iphy.ac.cn; http://iopscience.iop.org/cpb

**What follows is a list of articles you may be interested in**

---

## Lattice Boltzmann simulation on thermal performance of composite phase change material based on Voronoi models

Meng-Yue Guo(郭孟月), Qun Han(韩群), Xiang-Dong Liu(刘向东), and Bo Zhou(周博)
Chin. Phys. B, 2021, 30 (**10**): 104401. DOI: 10.1088/1674-1056/ac041d

## First-principles analysis of phonon thermal transport properties of two-dimensional $WS_2/WSe_2$ heterostructures

Zheng Chang(常征), Kunpeng Yuan(苑昆鹏), Zhehao Sun(孙哲浩), Xiaoliang Zhang(张晓亮), Yufei Gao(高宇飞), Xiaojing Gong(弓晓晶), and Dawei Tang(唐大伟)
Chin. Phys. B, 2021, 30 (**3**): 034401. DOI: 10.1088/1674-1056/abd2a6

## A phononic rectifier based on carbon schwarzite host-guest system

Zhongwei Zhang(张忠卫), Yulou Ouyang(欧阳宇楼), Jie Chen(陈杰), and Sebastian Volz
Chin. Phys. B, 2020, 29 (**12**): 124402. DOI: 10.1088/1674-1056/abbbf9

## Scaling behavior of thermal conductivity in single-crystalline $\alpha$-$Fe_2O_3$ nanowires

Qilang Wang(王啟浪), Yunyu Chen(陈允玉), Adili Aiyiti(阿地力·艾依提), Minrui Zheng(郑敏锐), Nianbei Li(李念北), Xiangfan Xu(徐象繁)
Chin. Phys. B, 2020, 29 (**8**): 084402. DOI: 10.1088/1674-1056/ab90f0

## A thermo-fluid analysis in magnetic hyperthermia

Iordana Astefanoaei, Ioan Dumitru, Alexandru Stancu, Horia Chiriac
Chin. Phys. B, 2014, 23 (**4**): 044401. DOI: 10.1088/1674-1056/23/4/044401

---

# Hierarchical lichee-like $Fe_3O_4$ assemblies and their high heating efficiency in magnetic hyperthermia*

Wen-Yu Li(李文宇)[1], Wen-Tao Li(李文涛)[4], Bang-Quan Li(李榜全)[1], Li-Juan Dong(董丽娟)[1], Tian-Hua Meng(孟田华)[1], Ge Huo(霍格)[3], Gong-Ying Liang(梁工英)[2], and Xue-Gang Lu(卢学刚)[2,†]

[1] *Institute of Solid State Physics, Shanxi Datong University, Datong* 037009, *China*
[2] *MOE Key Laboratory for Non-Equilibrium Synthesis and Modulation of Condensed Matter, School of Physics, Xi'an Jiaotong University, Xi'an* 710049, *China*
[3] *College of Material Science and Engineering, Shenzhen University, Shenzhen* 518061, *China*
[4] *No.* 93601 *Troops of PLA*

(Received 5 January 2021; revised manuscript received 20 March 2021; accepted manuscript online 3 June 2021)

A nontoxic and biocompatible thermoseed is developed for the magnetic hyperthermia. Two kinds of thermoseed materials: hierarchical hollow and solid lichee-like $Fe_3O_4$ assemblies, are synthesized by a facile hydrothermal method. The crystal structure of $Fe_3O_4$ assemblies are characterized by x-ray diffraction, scanning electron microscopy, and transmission electron microscopy. Moreover, the prepared $Fe_3O_4$ assemblies are used as a magnetic heat treatment agent, and their heating efficiency is investigated. Compared to solid assembly, hollow lichee-like $Fe_3O_4$ assembly exhibits a higher specific absorption rate of 116.53 W/g and a shorter heating time, which is ascribed to its higher saturation magnetization, larger initial particle size, and the unique hierarchical hollow structure. Furthermore, the magnetothermal effect is primarily attributed to Néel relaxation. Overall, we propose a facile and convenient approach to enhance the heating efficiency of magnetic nanoparticles by forming hollow hierarchical assemblies.

**Keywords:** magnetic hyperthermia, heating efficiency, hierarchical $Fe_3O_4$ assemblies

**PACS:** 44.10.+i, 87.85.J–, 75.75.–c **DOI:** 10.1088/1674-1056/ac0789

## 1. Introduction

Magnetic fluid hyperthermia (MFH) is an effective means of cancer treatment based on the magnetic nanoparticles (NPs).[1,2] In this process, magnetic NPs are locally injected into cancer tissues, which are then exposed to an external alternating magnetic field (AMF). This field causes the particles to reach therapeutic temperatures (42–46 °C), which eventually kills tumor cells.[3–5] MFH, with minimal side effects, provides a distinct advantage over other treatment methods such as chemotherapy and radiation therapy.[6] Owing to their excellent biocompatibility, biodegradability, magnetic targeting ability, and local heating ability in AMF, superparamagnetic iron oxide NPs have garnered considerable interest in tumor diagnosis and thermal therapy.[7–9] Several shapes of iron oxide NPs have been utilized as efficient heat mediators,[10–13] such as nanorods (NRs),[14] nanocubes,[15] and linear chains.[16] However, in the process of MFH, how to use less magnetic material and quickly reach the required treatment temperature in a short time is an important problem that needs to be solved. An ideal magnetic heat treatment agent should possess high heating efficiency as well as superparamagnetic properties to avoid magnetic reunion during the process of magnetic targeting.[17] Most superparamagnetic NPs obtained by traditional methods exhibit low heating efficiency due to their small particle size and low saturation magnetization ($M_s$).[18] Increasing the particle size is favorable for enhancing the $M_s$ of magnetic particles, which can increase the heating efficiency. However, the superparamagnetism of particles can be lost with the increase in particle size. This is not conducive to the targeted delivery of magnetic particles. To resolve this issue, $Fe_3O_4$ assemblies with hierarchical structure have been proposed, which possess a three-dimensional (3D) nanostructure. Owing to their unique properties, 3D nanostructures, typically formed using nanoparticles (0D), nanorods (1D), and nanoplates (2D) as building blocks, have attracted extensive attention.[19–23]

Meanwhile, although the magnetic properties of $Fe_3O_4$ NPs have been investigated,[24] and $Fe_3O_4$ NPs have been established as good materials for applications in MFH treatment,[25] the performance of hierarchical $Fe_3O_4$ hollow assemblies and solid assemblies in hyperthermia has been rarely compared in the existing literature. Further, it is noteworthy that the research on magnetothermal effect is essentially at a nascent stage based on the simple analysis of experimental results, and the heat generation mechanism of magnetic NPs with hierarchical structure has not been described yet.

In an earlier study, we proposed a simply controlled hydrothermal method[23] to prepare the superparamagnetic

*Project supported by the National Natural Science Foundation of China (Grant No. 61975162), Youth Research Foundation of Shanxi Datong University (Grant No. 2019Q1), Important R&D Projects of Shanxi Province, China (Grant No. 201803D121083), and Shanxi Scholarship Council, China (Grant No. 2020-135).

†Corresponding author. E-mail: xglu@xjtu.edu.cn

© 2021 Chinese Physical Society and IOP Publishing Ltd 

$Fe_3O_4$ NPs with 3D lichee-like hierarchical structure. In this work, the heating efficiency and magnetothermal mechanism of hierarchical hollow $Fe_3O_4$ assembly are examined, which are compared with those of solid assembly. The results reveal that the hollow assembly exhibits higher heating efficiency, higher saturation temperature, and a shorter heating time than solid assembly. This indicates that hierarchical hollow $Fe_3O_4$ assemblies with a unique monodisperse graded structure can serve as an excellent magnetic heat treatment agent in biomedical applications.

## 2. Experimental details

### 2.1. Synthesis of lichee-like hollow $Fe_3O_4$ assemblies

The simplest synthetic route to 3D hierarchical structure is self-assembly in which ordered aggregates are formed in a spontaneous manner. We use the hydrothermal method,[23] which is conducted in a high-temperature and high-pressure reaction environment. The hydrothermal method provides better control on the morphology and particle size distribution, and it is conducive to improving the magnetic properties and purity of the product. The details of the process are as follows: ferric chloride ($FeCl_3{\cdot}6H_2O$), sodium citrate, urea, and polyacrylamide (PAM) were obtained from Sigma-Aldrich. All the chemicals used were analytical grade. In a typical synthesis process, 0.27 g of $FeCl_3{\cdot}6H_2O$ was added to a round-bottom beaker containing 40 mL of deionized water, which was stirred for 10 min until the solution became yellow in color. Then, 0.88 g of sodium citrate, 0.36 g of urea, and 0.35 g of PAM were dissolved in the solution under mechanical stirring for 10 min. The experiment was performed under atmospheric air. After being magnetically stirred for 30 min at room temperature, the mixed solution was poured into a teflon-lined stainless steel autoclave with a capacity of 50 mL, which was then heated to and retained at 200 °C for 12 h. Subsequently, the autoclave was naturally cooled to room temperature, and the resulting black suspension was washed with distilled water and absolute ethanol. The precipitate was separated by centrifugation at 3000 rpm for 2 min, rinsed with absolute ethanol for several times, and dried in an oven at 60 °C for 6 h.

### 2.2. Characterization of material structure

The crystal structure of the studied sample was analyzed by x-ray diffraction (XRD). The morphology of products was investigated by scanning electron microscope (SEM), transmission electron microscopy (TEM), high-resolution TEM (HRTEM), and selected area electron diffraction (SAED).

### 2.3. Characterization of heating efficiency

The magnetic heating experiments were conducted using an AMF generated by a magnetic hyperthermia machine with a frequency of 55 kHz and field strength of 345 A/m. The experimental equipment is shown in Fig. 1. During the heating experiment, the sample holder was placed inside the coil, and the temperature rise was monitored using a thermometer.

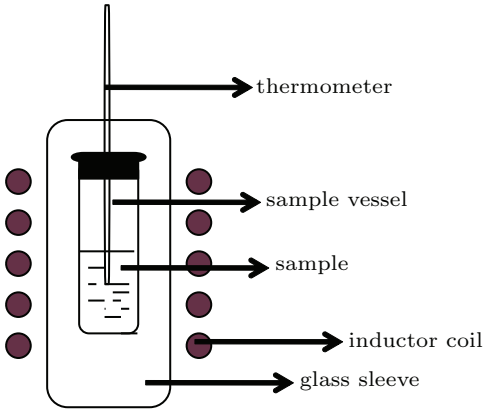



**Fig. 1.** Experimental equipment for measuring specific absorption rate.

## 3. Results and discussion

The SEM and TEM images of hollow and solid $Fe_3O_4$ assemblies are presented in Fig. 2. The SEM images in Figs. 2(a) and 2(b) demonstrate that the sample is composed of many initial NPs connecting with each other to form stable 3D lichee-like structures. Each assembly exhibits a hierarchical structure, while holes are observed in the individual assembly (inset of Fig. 2(b)), indicating the existence of porous structures. Figure 2(d) shows the TEM images of the samples, which is consistent with the SEM results that verify loose and porous structures. Moreover, the TEM image in the inset of Fig. 2(d) indicates that initial NPs are distributed on the periphery of the primary assembly, and a void is found in the center of the assembly, further validating the existence of porous and hollow structures. However, the TEM image in Fig. 2(c) indicates that the assembly is solid, and NPs are distributed on the entire assembly. In addition, according to the measurement results, the diameter of hollow $Fe_3O_4$ assemblies is about 160 nm, which are assembled by primary $Fe_3O_4$ crystals (mean diameter is nearly 18 nm). However, solid $Fe_3O_4$ assemblies (130 nm) consist of primary grains with a size of 16.5 nm.

The HRTEM image of hollow $Fe_3O_4$ assemblies is illustrated in Fig. 3(a). The lattice fringes are apparent with an interval of 0.295 nm, which is consistent with the lattice spacing of (220) plane of spinel-type $Fe_3O_4$. The lattice fringes of (400) plane of $Fe_3O_4$ agree with the $d$-spacing of 0.210 nm. Furthermore, the SAED pattern in Fig. 3(b) reveals the highly polycrystalline characteristic of $Fe_3O_4$, and the rings in the pattern can be indexed to (111), (220), (311), (400), (511), and (440) planes of spinel-type $Fe_3O_4$. The ring-like diffraction pattern suggests that the samples are composed of polycrystalline materials, which is consistent with the structure of

$Fe_3O_4$ (magnetite, JCPDS 19-0629). Overall, hierarchical hollow $Fe_3O_4$ assembly is porous, and has a low density and large specific surface area. Further, the hollow part can accommodate a large number of guest molecules, and cells and drugs can be easily adsorbed on its surface, so it can be widely used in the biomedical drug carriers.

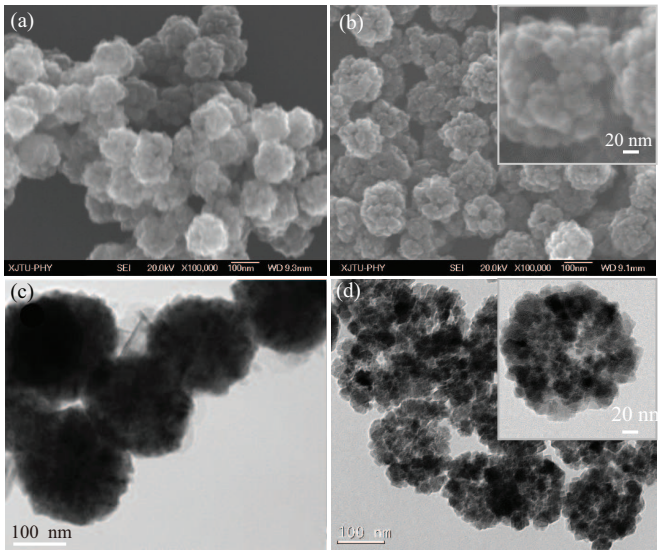



**Fig. 2.** SEM and TEM images of solid $Fe_3O_4$ assemblies (heated for 8 h; (a), (c)) and hollow $Fe_3O_4$ assemblies (heated for 12 h; (b), (d)). The insets in (b) and (d) show SEM and TEM images of a single hollow $Fe_3O_4$ assembly, respectively.

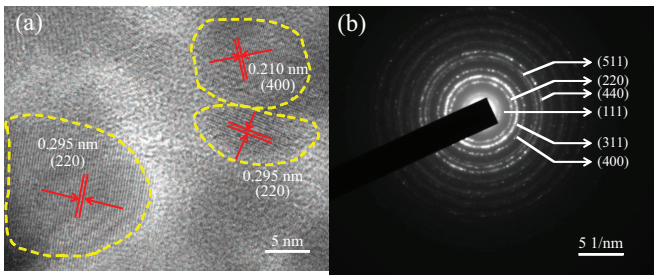



**Fig. 3.** (a) HRTEM image and (b) SAED pattern of hollow $Fe_3O_4$ assemblies.

Figure 4 shows the XRD patterns of the prepared assemblies. All the characteristic XRD peaks correspond to face centered cubic (FCC) structure of $Fe_3O_4$. Almost no XRD peaks for impurity phases can be observed, which proves the high crystallinity of the samples prepared using the proposed hydrothermal method. All the diffraction peaks can be attributed to the spinel-type $Fe_3O_4$. In addition, we calculate the crystallite size ($d$) using the following Scherrer equation: $d = \kappa\lambda/B\cos\theta$, where $B$ is the full-width-at-half-maximum (FWHM) of the XRD peak, $\theta$ is the diffraction angle corresponding to the peak, and $\lambda$ is the wavelength of the x-ray beam. Using the FWHM of the strongest diffraction peak at $2\theta = 35.6°$, the size of grains can be calculated as 18.5 nm and 16.8 nm, which are in good agreement with the diameters of small primary grains. Obviously, it is also proved that the synthesized lichee-like $Fe_3O_4$ assemblies are composed of primary grains and have a unique hierarchical structure.

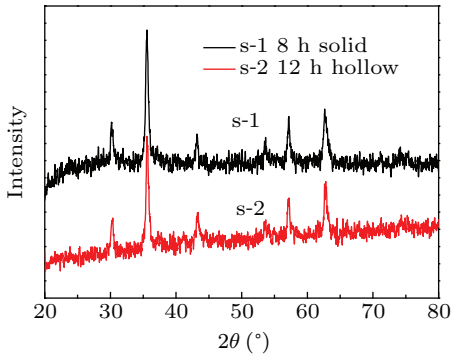



**Fig. 4.** XRD patterns of the prepared assemblies.

The magnetic properties of hollow and solid $Fe_3O_4$ assemblies at room temperature were investigated by our group in Ref. [23]. The hysteresis loops indicate that both the samples exhibit typical superparamagnetic behavior without coercivity. As reported before,[23] compared to the solid assembly, the hollow assembly has a higher $M_s$ (73.3 emu/g). Figure 5 shows the variation in coercivity as a function of particle size. It is well known that reducing the size of magnetic particles can lead to the formation of single-domain particles, which causes superparamagnetism.[26–28] When the size of magnetic particles is below 20 nm, the transformation from ferromagnetic to superparamagnetic behavior occurs. Magnetic NPs display superparamagnetism, i.e., they do not remain magnetized under an external AMF, preventing particle aggregation.[2] It is noteworthy that the assemblies exhibit superparamagnetic characteristic and have high $M_s$, which may govern the heating power in magnetic heating experiments. Therefore, the hierarchical lichee-like $Fe_3O_4$ assemblies can be used as thermoseeds for local MFH treatment of cancers.

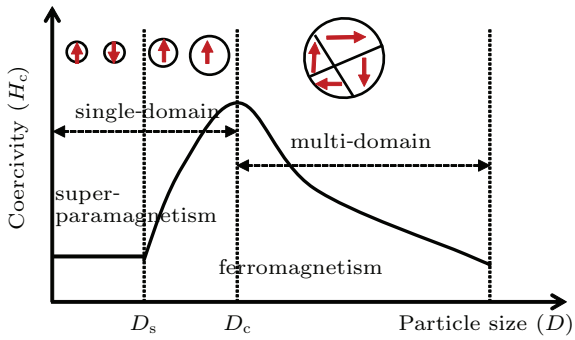



**Fig. 5.** Relationship between particle size and coercivity. $D_s$ and $D_c$ represent the 'superparamagnetism' and 'critical' size thresholds.

When magnetic nanoparticles are subjected to an alternating magnetic field, in the process of repeated magnetization, they absorb a large amount of electromagnetic wave energy and convert it into heat through hysteresis loss, and relaxation loss, etc. This heat generation process is called magnetothermal effect. It is generally believed that in the low and intermediate frequency range, the loss mechanism of micron-sized magnetic particles is mainly hysteresis loss, while the loss of

superparamagnetic particles is primarily caused by relaxation loss. The relaxation loss can be expressed as

$$P = \pi\mu_0\chi_0 H^2 f \frac{2\pi f\tau}{1+(2\pi f\tau)^2}, \tag{1}$$

where $\mu_0$ is the permeability of free space, $H$ and $f$ are the amplitude and frequency of the AC field, respectively. $\chi_0$ is a magnetic-field-dependent parameter, which is defined as

$$\chi_0 = \chi_{\rm i}\frac{3}{\xi}\left(\coth(\xi)-\frac{1}{\xi}\right), \tag{2}$$

where $\xi$ is the Langevin parameter ($\xi = \mu_0 M_{\rm s} HV/kT$, $M_{\rm s}$ is the domain magnetization of a suspended particle). The initial susceptibility $\chi_{\rm i}$ is determined from the differentiation of the Langevin relationship.[3] Evidently, the heating of the magnetic nanoparticles is not only related to the amplitude $H$ and frequency $f$ of the AC magnetic field but also strongly depends on the physical properties of the materials, such as the particle size and shape as well as the microstructure. Figure 6 shows the variation in temperature of the samples as a function of heating time for particle concentration of 10 mg/mL and 5 mg/mL. These curves are obtained using an in vitro experiment of rise in temperature under an AMF of 55-kHz frequency and different input powers (3.0 kW, 4.5 kW, 6.0 kW). In all the experiments, the assemblies were heated from room temperature to the highest heating temperature before they were allowed to cool. It is evident in Fig. 6 that when the sample concentration is 10 mg/mL, the temperature shows an increasing trend under different powers, and the rate of temperature rise is larger during the early stage of heating, which gradually reduces, and finally a stable temperature is reached. The slope of magnetocaloric curves of the magnetic assemblies is different under different powers, and the highest temperature value is also different. Figure 6 reveals that the hollow $Fe_3O_4$ assemblies with concentration of 10 mg/mL and 5 mg/mL reach a maximum temperature of 60.8 °C and 41.2 °C, respectively, at input power of 4.5 kW. Obviously, the required treatment temperature (42–46 °C) is reached in 2 min when the concentration is 10 mg/mL. After nearly 7 min, the sample reaches saturation temperature. Because the heat generated by the magnetic material finally balances with the heat dissipated outside, it reaches the saturation temperature and no longer changes. It is evident from the figures that the saturation temperature and rate of temperature rise are highly dependent on the concentration of assemblies, and they basically show a positive correlation (as shown in Tables 1 and 2).

The efficiency of the heat generation by the magnetic nanoparticles is expressed using specific absorption rate (SAR) with units of W/g, which provides a measure of the rate at which energy is absorbed per unit mass of the magnetic particles when they are exposed to an alternating magnetic field.[15] It is expressed as (using magnetite as an example) follows:

$$\mathrm{SAR} = C\frac{\Delta T}{\Delta t}\frac{1}{m_{\rm Fe}}, \tag{3}$$

where $C$ is the specific heat capacity and $m_{\rm Fe}$ is the mass of Fe in $Fe_3O_4$ NPs.[6,13] $\Delta T/\Delta t$ is the initial rate of the temperature rise. The SAR value provides a measure of the heat performance of magnetic NPs.[29] The SAR value, saturation temperature, duration, and initial heating rate of the magnetic assemblies under different input powers and various concentrations are shown in Tables 1 and 2. When the power is 3.0 kW and the concentration is 10 mg/mL, the maximum temperature of magnetic solution is 53.0 °C, which is less than the temperature at 4.5 kW and 6.0 kW. Further, the required heating time for the former case is longer, and the SAR value is much less than that obtained under other two conditions. When the power is 4.5 kW, the maximum temperature is 60.8 °C, and the SAR value is 116.53 W/g, which is much higher than that of $Fe_3O_4$ with other morphologies and sizes reported in Ref. [3].

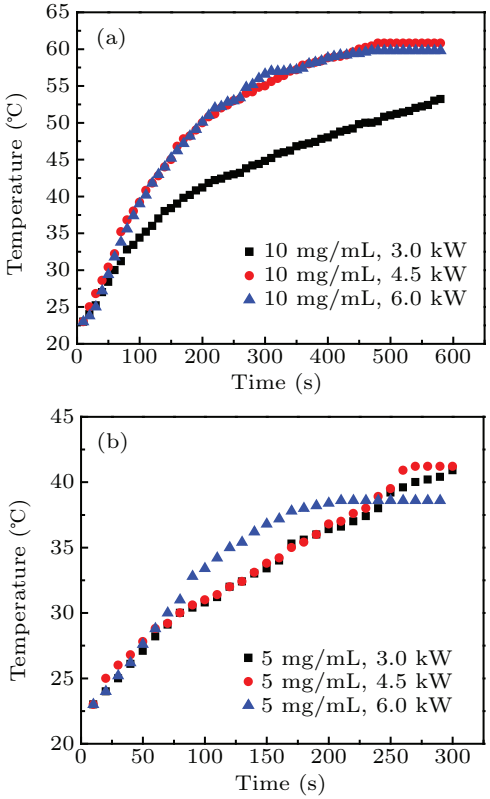



**Fig. 6.** Variation in the temperature as a function of heating time for different powers in an external AMF with frequency of 55 kHz [(a) particle concentration = 10 mg/mL, (b) particle concentration = 5 mg/mL].

**Table 1.** SAR, saturation temperature, duration, and initial heating rate under different input powers with concentration of 10 mg/mL.

| Input power (kW) | 3.0 | 4.5 | 6.0 |
|---|---|---|---|
| SAR values (W/g) | 79.06 | 116.53 | 104.13 |
| Saturation temperature (°C) | 53.0 | 60.8 | 59.8 |
| Duration (s) | 580 | 500 | 490 |
| Initial heating rate (°C/min) | 4.0 | 5.6 | 4.2 |

**Table 2.** SAR, saturation temperature, duration, and initial heating rate under different input powers with concentration of 5 mg/mL.

| Input power (kW) | 3.0 | 4.5 | 6.0 |
|---|---|---|---|
| SAR values (W/g) | 71.31 | 111.72 | 71.62 |
| Saturation temperature (°C) | 40.9 | 41.2 | 38.6 |
| Duration (s) | 320 | 290 | 250 |
| Initial heating rate (°C/min) | 3.1 | 3.8 | 3.2 |

To understand the influence of hollow and solid $Fe_3O_4$ assemblies on the magnetothermal properties, *in vitro* experiments for the evaluation of temperature rise were conducted. Figure 7 shows the time dependence of heating temperature of the hollow and solid $Fe_3O_4$ assemblies with particle concentration of 10 mg/mL and 5 mg/mL under an AMF with a frequency of 55 kHz and input power of 4.5 kW. The SAR value is widely used to characterize the heat generation capability of magnetic nanoparticles. However, for a better comparison, we also propose the intrinsic loss power (ILP) to normalize the SAR value, which is calculated as follows:[10]

$$\mathrm{ILP} = \frac{\mathrm{SAR}}{H^2 f}, \tag{4}$$

where $H$ is the strength of the magnetic field and $f$ is the frequency. The SAR, ILP, saturation temperature, and initial heating rate of the magnetic assemblies under different concentrations are shown in Table 3. It is clear that higher concentration leads to a larger increase in temperature. Comparing the two types of assemblies, it can be observed that the heating effect of hollow $Fe_3O_4$ assemblies is better than that of solid $Fe_3O_4$ assemblies. For example, hollow $Fe_3O_4$ assemblies with concentration of 10 mg/mL need 2.2 min to reach a temperature of 42 °C, while the solid $Fe_3O_4$ assemblies require 3.7 min to reach this temperature under the same condition. The SAR and maximum temperature rise of hollow $Fe_3O_4$ assemblies at different concentrations are higher than that of solid assemblies. Compared to the SAR of solid $Fe_3O_4$ assemblies (SAR = 79.06 W/g), the measured SAR of hollow $Fe_3O_4$ (SAR = 116.53 W/g) is much higher under the same conditions. Besides, in addition to high SAR, hollow $Fe_3O_4$ assemblies have a higher initial heating rate, and they require a shorter time to reach the saturation temperature. For hollow $Fe_3O_4$, ILP = 17800, which is higher than that of the solid assembly and is sufficiently high for hyperthermia application. This indicates that the hierarchical hollow lichee-like $Fe_3O_4$ assemblies have strong heat production capacity and excellent magnetothermal performance. When the concentration is 10 mg/mL, the temperature of hollow $Fe_3O_4$ increases from 23 °C to 60.8 °C in a duration of 500 s. When the temperature reaches 60.8 °C, the temperature gradually tends to be stable, and the average heating rate is nearly 4.6 °C/min. Due to the *in vivo* heat balance effect, the initial temperature of magnetic NPs is 37 °C. To reach the tumor treatment temperature of 42–46 °C, the heating time of magnetic NPs is only 1–2 min. From the perspective of clinical treatment, this heating rate of magnetic NPs is helpful to improve the treatment efficiency and reduce the side effects on normal tissues and cells caused by long-term heating. In addition, high magnetothermal temperature can also meet the requirements of clinical thermal ablation.

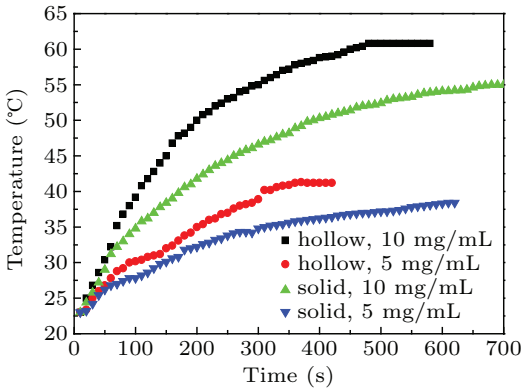



**Fig. 7.** Variation in the temperature as a function of heating time for hollow and solid $Fe_3O_4$ assemblies under an AMF with frequency of 55 kHz.

**Table 3.** SAR, ILP, saturation temperature, and initial heating rate of magnetic assemblies with different concentrations.

| Morphology | Hollow/Solid | Hollow/Solid |
|---|---|---|
| Concentration (mg/mL) | 10 | 5 |
| SAR (W/g) | 116.53/79.06 | 111.72/71.31 |
| ILP (nHm$^2$/kg) | 17800/12076 | 17065/10893 |
| Saturation temperature (°C) | 60.8/55.0 | 41.2/38.4 |
| Initial heating rate (°C/min) | 5.6/4.2 | 3.8/2.4 |

It is well known that two relaxation mechanisms can occur for magnetic fluids: Néel relaxation and Brownian relaxation. Néel relaxation represents the fluctuations that arise from the jumps of magnetic moment between different easy directions. Brownian relaxation characterizes the viscous rotation of all the particles.[28] Because the size of primary grains of $Fe_3O_4$ assemblies are below the critical size of monodomain particles and these grains are connected and clustered, the Brownian rotation of the grains under an external magnetic field is limited. Therefore, the possibility of heat generation by Brownian relaxation is relatively low. The generation of heat in the assemblies can only be realized by the rotation of the magnetic moment of primary grains under AMF. In other words, for the synthesized hierarchical $Fe_3O_4$ assemblies, the heat is most likely generated through Néel relaxation. However, the thermal efficiency of hollow $Fe_3O_4$ assembly is higher than that of solid $Fe_3O_4$ assembly due to the following reasons. Firstly, the $M_s$ of hollow assemblies is higher than that of solid assemblies. This implies that the magnetic moment per unit volume is higher, and the rotational thermal efficiency of hollow aggregates under the external AMF is higher. Secondly, because of its unique hollow structure, the contact area between hollow particles and solution is larger in the in vitro temperature rise experiment. Consequently, the

heating is more uniform, which is conducive to the rise in temperature. In addition, as shown in Figs. 2(a) and 2(b), compared to the solid assemblies, hollow assemblies have a loose and porous structure, large specific surface area, and exhibit good dispersibility in the solution, while the solid assemblies are more compact and have poor dispersibility. Due to these characteristics, the transfer of heat generated by hollow samples into the solution is faster and more effective. Because the hollow assemblies have a loose porous structure with gaps between some primary grains, it can be inferred that the heat production in the hollow structure is mainly caused by Néel relaxation, but there is a small contribution of Brownian relaxation. These results indicate that the hierarchical lichee-like hollow $Fe_3O_4$ assemblies may be an ideal thermoseed for MFH. Overall, by forming a hierarchical hollow structure, we establish an effective way to enhance the heating efficiency of magnetic nanoparticles. The superparamagnetic properties of the primary grains are retained, which is beneficial to the targeted transport in an organism. At the same time, the hollow part can hold a large number of guest molecules and can be used as a drug carrier. More importantly, the primary grains are stacked on each other to form larger spherical assemblies, which causes an increase in the saturation magnetization and facilitates their application in magnetic hyperthermia.

## 4. Conclusions

In this study, two kinds of iron oxide materials: hierarchical hollow and solid lichee-like $Fe_3O_4$ assemblies, were used as thermoseeds for MFH, and their magnetothermal effect was investigated. It was found that the hollow $Fe_3O_4$ assemblies displayed higher heating efficiency, and their SAR reached up to 116.53 W/g. Hyperthermia experiments revealed that hollow $Fe_3O_4$ magnetic fluid assembly could reach a maximum heating temperature of 60.8 °C and the average heating rate was 4.6 °C/min. Further, it was demonstrated that the unique loose porous hierarchical structure of particles could improve the contact area between hollow assemblies and solution and also induced gaps between some primary grains. These results indicated $M_s$ is not an only parameter to optimize the SAR, and the heating efficiency of magnetic thermoseeds can be enhanced by changing the arrangement of NPs. Furthermore, the high heat production of hollow $Fe_3O_4$ assemblies was mainly attributed to Néel relaxation with a small contribution of Brownian relaxation.

## References


[1] Liu R T, Liu J, Tong J Q, Tang T, Kong W C, Wang X W, Li Y and Tang J T 2012 *Progress in Natural Science: Materials International* **22** 31

[2] Sharifi I, Shokrollahi H and Amiri S 2012 *J. Magn. Magn. Mater.* **324** 903

[3] Zhang L Y, Gu H C and Wang X M 2007 *J. Magn. Magn. Mater.* **311** 228

[4] Ling Y, Tang X Z, Wang F J, Zhou X H, Wang R H, Deng L M, Shang T T, Liang B, Li P, Ran H T, Wang Z G, Hu B, Li C H, Zuo G Q and Zheng Y Y 2017 *RSC Adv.* **7** 2913

[5] Hao H Q, Ma Q M, He F and Yao P 2014 *J. Mater. Chem. B* **2** 7978

[6] Zhao L Y, Tang J T and Feng S S 2010 *Nanomedicine* **5** 1305

[7] Cho M J, Cervadoro A, Ramirez M R, Stigliano C, Brazdeikis A, Colvin V L, Civera P, Key J and Decuzzi P 2017 *Nanomaterials* **7** 72

[8] Zhao L Y, Liu J Y, Ouyang W W, Li D Y, Li L, Li L Y and Tang J T 2013 *Chin. Phys. B* **22** 108104

[9] Yu Y K and Sun D X 2010 *Expert Rev. Clin. Pharmacol.* **3** 117

[10] Nikitin A, Khramtsov M, Garanina A, Mogilnikov P, Sviridenkova N, Shchetinin I, Savchenko A, Abakumov M and Majouga A 2019 *J. Magn. Magn. Mater.* **469** 443

[11] Yang Y X, Huang M W, Qian J M, Gao D Q and Liang X L 2020 *Sci. Rep.* **10** 8331

[12] Kolen'ko Y V, Banobre-Lopez M, Rodriguez-Abreu C, Carbo-Argbay E, Sailsman A, Pineiro-Redondo Y, Cerqueira M F, Petrovykh D, Kovnir K, Lebedev O I and Rivas J 2014 *J. Phys. Chem. C* **118** 8691

[13] Tong S, Quinto C A, Zhang L L, Mohindra P and Bao G 2017 *Acs Nano* **11** 6808

[14] Geng S, Yang H T, Ren X, Liu Y H, He S L, Zhou J, Su N, Li Y F, Xu C M, Zhang X Q and Cheng Z H 2016 *Chem. Asian. J.* **11** 2996

[15] Guardia P, Corato R D, Lartigue L, Wilhelm C, Espinosa A, Garcia-Hwenandez M, Gazeau F, Manna L and Pellegrino T 2012 *Acs Nano* **6** 3080

[16] Myrovali E, Maniotis N, Makridis A, Terzopoulou A, Ntomprougkidis V, Simeonidis K, Sakellari D, Kalogirou O, Samaras T, Salikhov R, Spasova M, Farle M, Wiedwald U and Angelakeris M 2016 *Sci. Rep.* **6** 37934

[17] Duguet E, Vasseur S, Mornet S, Goglio G, Demourgues A, Portier J, Grasset F, Veverka P and Pollert E 2006 *Bull Mater. Sci.* **29** 581

[18] Yang X Y, Zhang X Y, Ma Y F, Huang Y, Wang Y S and Chen Y S 2009 *J. Mater. Chem.* **19** 2710

[19] Li X Y, Si Z J, Lei Y Q, Li X N, Tang J K, Song S Y and Zhang H J 2011 *Crystengcomm* **13** 642

[20] Zhong L S, Hu J S, Liang H P, Cao A M, Song W G and Wan L J 2006 *Adv. Mater.* **18** 2426

[21] Lu X G, Huo G, Liu X L, Liang G Y, Han Z J and Song X P 2012 *Crystengcomm* **14** 5622

[22] Whitesides G M and Boncheva M 2002 *Proc. Natl. Acad. Sci.* **99** 4769

[23] Li W Y, Huo G, Huang Y, Dong L J and Lu X G 2018 *Acta Phys. Sin.* **67** 177501 (in Chinese)

[24] Han L, Li S Y, Yang Y, Zhao F M, Huang J and Chang J 2008 *J. Biomater. Appl.* **22** 433

[25] Timko M, Dzarova A, Kovac J, Skumiel A, Jozefczak A, Hornowski T, Gojzewski H, Zavisova V, Koneracka M, Sprincova A, Strbak O, Kopcansky P and Tomasovicova N 2009 *J. Magn. Magn. Mater.* **321** 1521

[26] Mathew D S and Juang R S 2007 *Chem. Eng. J.* **129** 51

[27] Dave S R and Gao X H 2009 *WIREs Nanomedicine and Nanobiotechnology* **1** 583

[28] Laurent S, Dutz S, Häfeli U O and Mahmoudi M 2011 *Adv. Colloid Interface Sci.* **166** 8

[29] Rosensweig R E 2002 *J. Magn. Magn. Mater.* **252** 370